Electron Measurement in PHENIX

Y. Akiba[a]

[a]Institute for Nuclear Study, University of Tokyo,
Midori-cho 3-2-1, Tanashi, Tokyo 188, Japan

Electron Measurement in PHENIX detector at RHIC is discussed. The yield and S/N ratio at vector meson peaks (ϕ, ω, ρ^0, and J/ψ) are evaluated. The electrons from open charm decay, and its consequence to the di-electron measurement is discussed.

1. INTRODUCTION

PHENIX [1] is one of the two major experiments of Relativistic Heavy Ion Collider (RHIC), now being constructed at Brookhaven National Laboratory. The experiment aims to study Au+Au collisions at $\sqrt{s} = 200$ GeV per nucleon, and to search for the phase transition from normal nuclear matter to quark-gluon plasma (QGP). The detector measures electrons, photons, and hadrons in the central detector, and measures muons in the forward muon arm. In this talk, we discuss electron measurement in PHENIX central detector. Other aspects of the experiment are presented in this workshop [2–4].

2. PHENIX Central Detector

PHENIX central detector is made of an axial field magnet and two almost identical arms placed left and right of the magnet. Each arm covers $\pm$ 0.35 units of pseudo-rapidity and 90 degrees in azimuthal angle. They are separated by 67.5 degrees in ϕ. A beam view of the PHENIX central arm is shown in figure 1.

Each arm is made of several detector subsystems. From the beam line, there is an inner tracking system made of 2 sets of drift chambers and a pad chamber. The inner tracker is followed by a Ring Image Cherenkov Detector (RICH), which provides electron/hadron separation from a few hundred MeV/c to about 4 GeV/c. Outside of the RICH detector is an outer tracking system made of a Time Expansion Chamber (TEC) sandwiched by two pad chambers. The TEC have a electron/hadron separation capability by a fine sampling dE/dx measurement. The last layer of the detector is an electromagnetic calorimeter (EMCAL) for photon measurement and for electron/hadron separation. A quarter of EMCAL is lead-glass calorimeter, and three quarter is Pb-Scintillator sampling calorimeter. The Pb-scintillator calorimeter have a good time of flight (TOF) capability that is useful for e/π separation at low energies. A part of one arm is equipped with high resolution TOF counters for hadron identification, but we will not discuss it here.

Electron identification is provided by the following three subsystems: RICH, TEC, and EMCAL. The RICH detector is a gas Cherenkov counter with 5120 PMT read-

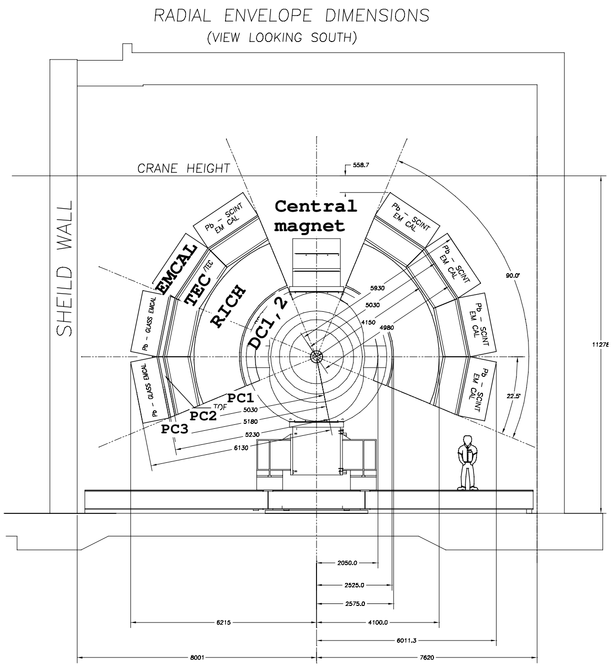

Figure 1. A beam view of PHENIX central detector.

out, and the main electron identification device in PHENIX central detector. The high segmentation of the read-out is required to uniquely associate Cherenkov light signals to tracks measured by the tracking system. A beam test of a small prototype of the device shows that it has a pion rejection better than 10^4 with electron acceptance > 99 % for a single isolated track. However, this excellent e/π rejection is reduced in a high particle density environment expected in RHIC Au+Au central collision because of ambiguities in association of Cherenkov signals with particle tracks. From a detailed GEANT Monte Carlo simulation, it is estimated that its e/π separation in Au+Au central collision is about 10^3. The TEC provides e/π separation by its dE/dx measurement. A beam test shows that its pion rejection factor is about 10^2 for a single isolated track with momentum < 2 GeV/c. The EMCAL provides about factor 10^2 pion rejection for tracks with momentum > 1 GeV/c. Combining all three subsystems, the PHENIX central arm has e/π separation better than 10^4 from a few hundred MeV/c to 4 GeV/c.

The acceptance of the detector is $dYd\phi = 0.7\pi$ for single e^+ or e^-, and about 4 % of $\frac{d\sigma}{dy}$ for e^+e^- pairs. The acceptance for the pair depends on $\frac{m}{p_t}$ of the pair.

One of the important design goals of the PHENIX central detector is high mass resolution to detect changes in properties of vector mesons in high energy density created in Au+Au central collisions. The expected mass resolution for J/ψ and ϕ as a function of transverse momentum is shown in figure 2. Mass resolution for ϕ is expected better than 4 MeV in r.m.s, which is comparable to its natural width ($\Gamma = 4.4$ MeV)[5]. The resolution gives us a high sensitivity to detect the changes in mass and width of ϕ if such

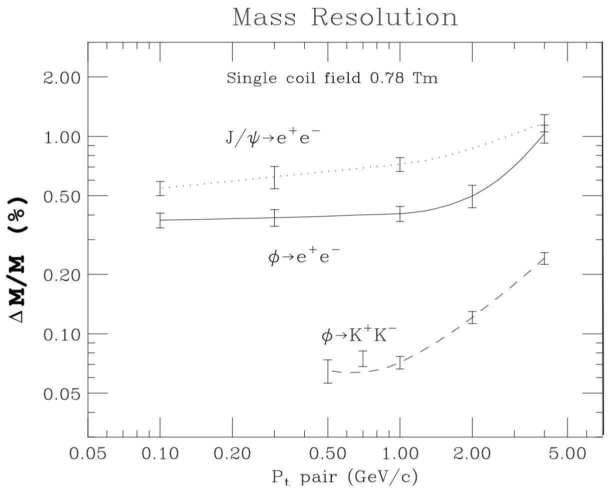

Figure 2. Mass resolution in PHENIX central detector.

changes occur in heavy ion collisions at RHIC.

3. Light Vector Mesons

There are many theoretical predictions on how the properties of light vector mesons (mass, width, and branching ratios of ρ, ω, and ϕ) can be changed in high density and/or high temperature state [6–21]. Measurement of light vector mesons through its leptonic decay mode is particularly useful to detect such changes, since we can probe the state of vector mesons deep inside the high density/temperature matter without the complication of final state interactions.

Figure 3 shows an expected di-electron mass spectrum measured in PHENIX central detector. The figure corresponds to 32 M central Au+Au collisions, roughly one week of data taking with nominal RHIC luminosity of $L = 2 \times 10^{26} cm^{-2}s^{-1}$. This is based on a full GEANT simulation of the detector that includes all backgrounds coming from shower particles in magnet yoke, gamma conversions in beam pipe, Dalitz decays of π^0. The particle tracks are reconstructed from hit positions in the tracking chambers, and electrons/positrons are identified from simulated responses of RICH and EMCAL detector. The figure is before background subtraction.

The broad continuum of dilepton spectrum are mostly combinatorial backgrounds from π^0 Dalitz decays and gamma conversions in beam pipe with small contributions from misidentified hadrons. The conversion in MVD (Multiplicity Vertex Detector), which surrounds the beam pipe, is not included in the simulation. If it is included, the background level increases by about 60 % [25]. Although backgrounds are large, we can clearly see signals of narrow vector mesons, ϕ and ω, above the background. We can also see J/ψ and $\psi(2S)$ in high mass region. However, ρ^0 resonance is buried in the background because of its broad width ($\Gamma = 151$ MeV[5]).

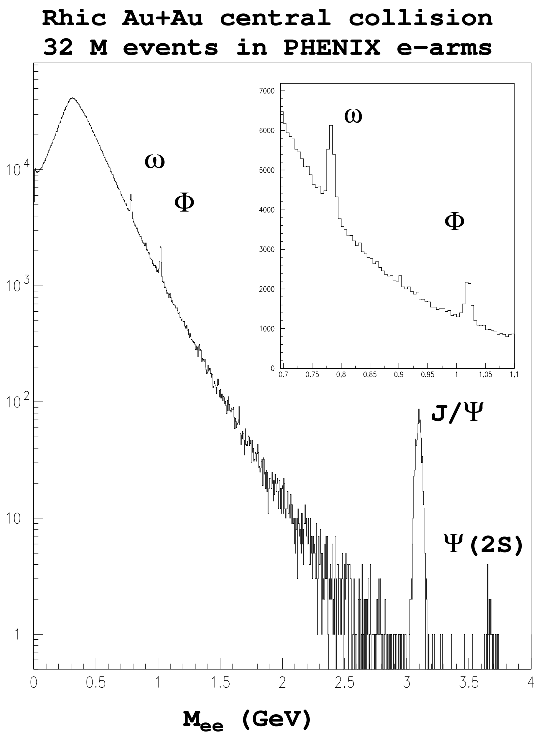

Figure 3. Mass spectrum of di-electrons in PHENIX central detector.

Expected yield of light vector mesons measured in PHENIX central arms in one year is summarized in table 1. Here we assume that the luminosity of RHIC is $L = 2 \times 10^{26} cm^{-2}s^{-1}$ for Au+Au, and one year is 3000 hours ($= 1.08 \times 10^8$ sec) of data taking. Assuming that we collect all central collision event (10 % of minimum bias event), we have about 1 G central events per year. In this calculation, we assume the following particle yield ratios: $\frac{N_{\rho^0}}{N_{\pi^0}} = 20$ %, $\frac{N_\omega}{N_{\rho^0}} = 1.0$, and $\frac{N_\phi}{N_{\pi^0}} = 2$ %. Those yield ratios are based on p+p data at the ISR [26].

Table 1
Yield of vector mesons and S/N ratios in one year of measurement in PHENIX central detector

	Yield (per year)	Background	S/N ratio	(Background)$^{1/2}$
ρ	110K	3.9M	1/35	2K
ω	170K	500K	1/3	0.7K
ϕ	75K	150K	1/2	0.4K

As one can see from the figure 3 as well as table 1, we have a reasonable S/N ratio and large statistics for measurement of ω and ϕ. For ρ^0, the S/N ratio is rather poor (S/N $\sim$ 1/35). Although in principle we have enough statistic after the background subtraction, we need to understand the background shape very well to extract the signal.

We want to note that the reason we expect a poor S/N ratio for ρ^0 is that we use a conservative estimate for the ρ^0 production cross section, a simple scaling of particle ratio from p+p collisions. In nucleus-nucleus collisions at RHIC energies, it is expected that a mixed phase state or a hot hadronic gas is formed with a long life time ($\sim$ 10 fm/c). Since life time of ρ is short ($c\tau$ = 1.2 fm), they are formed for several generations by $\pi\pi \rightarrow \rho^0$reaction in this high energy density / high temperature state [24]. Therefore the yield of $\rho^0 \rightarrow e^+e^-$ can be larger than that of simple scaling from p+p collisions used in our yield estimation unless the life time of the "fireball" is short or ρ^0 is desolved in the hot dense matter. In other words, in table 1, we neglect the contribution of $\pi\pi \rightarrow \rho^0 \rightarrow e^+e^-$ reaction, and thus the yield and S/N ratio of ρ in the table should be considered as a conservative minimum value.

4. J/ψ Measurement

"Suppression" of J/ψ is one of the proposed signals of quark gluon plasma formation[27], and such "suppression" has been observed in di-muon experiment at the CERN SPS [28]. It is, therefore, very important to measure J/ψ at RHIC energy.

As show in figure 3, we have an excellent S/N ratio for J/ψ measurement because of high mass resolution of the detector. The measurement is limited by a rather small solid angle of the detector, whose acceptance is about 4 % of dN/dy for J/ψ. The expected yield of J/ψ and ψ(2S) detected in PHENIX central arms are summarized in table 2. Here we assume that the cross section $\frac{B_{ee}d\sigma}{dy}$ $(pp \rightarrow J/\psi)$ is 50 nb [30,31] at $\sqrt{s}$ = 200 GeV, and that the cross section scales as $\sigma(AA) \propto A^{2\alpha}$ with $\alpha = 0.92$[29,32]. In other words, we do not include additional "J/ψ suppression" other than observed in pA collisions in this estimate.

Table 2
Yield of J/ψ ψ(2S) in one year of measurement in PHENIX central detector

	Yield (minimum bias)	Yield (central)
J/ψ	70K/year	14K/year
ψ(2S)	1.4K/year	300/year

J/ψ cross section should be measured for a wide range of transverse momentum to clarify the "suppression mechanism", that is, to distinguish the "suppression" in normal nuclear matter and that in quark gluon plasma. Therefore, it is worthwhile to evaluate how high in p_t we can measure J/ψ in PHENIX central detector.

There are a few measurement of $pp(p\bar{p}) \rightarrow J/\psi$ at high transverse momentum.

$\sqrt{s} = 63$ GeV (pp) $\quad \frac{B_{ee}d\sigma}{dy} \simeq 5$ pb ($p_t \geq 5$ GeV/c)[33]

$\sqrt{s} = 630$ GeV $(p\bar{p})$ $\quad \frac{B_{\mu\mu}d\sigma}{dy} \simeq 1.7$ nb ($p_t \geq 5$ GeV/c) [34]

$\sqrt{s} = 1.8$ TeV ($p\bar{p}$) $\quad \frac{B_{\mu\mu} d\sigma}{dy} \simeq 6.9$ nb ($p_t \geq 6$ GeV/c) [35]

From those values, we estimate that $\frac{Bd\sigma}{dy}$ ($pp \rightarrow J/\psi$) $\simeq 200$ pb for $p_t \geq 5$ GeV/c at $\sqrt{s} = 200$ GeV. To scale this cross section to Au+Au collisions, we use nuclear dependence slope $\alpha = 1.0$, since there will be less nuclear effect in high p_t region. The acceptance of PHENIX central detector for high p_t J/ψ is about 2 % of dN/dy. We expect about 300 (60) events above $p_t \geq 5$ GeV/c for minimum bias (central) Au+Au collisions in one year. This means that we can measure J/ψ cross section up to ~ 6 GeV/c, where "J/ψ suppression" in the QGP model becomes small[36].

Strictly speaking, we are not measuring the "J/ψ suppression" in this high transverse momentum region, since most of the J/ψ's above 5 GeV/c in p_t are decay product of χ_c meson[37]. However, since p_t dependence of "suppression" of χ_c in the QGP model is similar to that of J/ψ[36], the measurement of high p_t is useful to clarify the suppression mechanism.

5. Charm and single electrons

Enhanced production of charm is proposed as a "signature" of QGP[38], and charm production is proposed as a sensitive "thermometer" and a "probe" [39,40] of the early stage of nucleus-nucleus collisions. If there is an enhanced production of charm in nucleus-nucleus collisions, such phenomena can be observed as an enhanced production of "single electron" in $p_t = 1$ to 5 GeV/c. Open charm is also a major source of background for dilepton continuum measurement [41]. Therefore, it is very important to evaluate the charm production at RHIC, and its consequence to electron measurement.

Here we briefly summarize the charm production at RHIC energy. There are several measurements of hadronic charm production at SPS and FNAL fixed target energies. They showed that $\sigma(pp \rightarrow c\bar{c})$ is about 15 μb at $\sqrt{s} = 28$ GeV [42], and 20 to 40 μb at $\sqrt{s} = 40$ GeV[43–46]. Perturbative QCD calculations predict that charm production cross section $\sigma(pp \rightarrow c\bar{c})$ increases by factor 5 to 10 from $\sqrt{s} = 40$ to 200 GeV [47–49]. Although there is uncertainty in pQCD calculations of charm production, which depends on the choice of gluon distribution function, the mass of c-quark, and the normalization scale, it is generally agreed that the charm cross section $\sigma(pp \rightarrow c\bar{c})$ is 150 to 250 μb at RHIC energy ($\sqrt{s} = 200$ GeV)[48–50].

To scale this elementary cross section to nucleus-nucleus collision, we need the nuclear dependence α, defined as $\sigma(pA) \propto A^{\alpha}$. Recent measurement of $p + A \rightarrow D\bar{D}$ at FNAL shows that $\alpha_{D\bar{D}} = 1.02 \pm 0.03 \pm 0.02$ near center-of-mass rapidity[44]. This behavior is consistent with charm production by gluon fusion model ($gg \rightarrow c\bar{c}$), if nuclear shadowing of gluons can be neglected. There is a theoretical estimates that charm production at RHIC Au+Au central collisions is reduced by 30 % [50]to 50 % [39,51] from the value of $\alpha_{c\bar{c}} = 1.0$ by nuclear shadowing. On the other hand, there are theoretical predictions that charm pairs produced in "pre-equilibrium stage" in Au+Au central collisions is comparable to that of initial pQCD production [39,40]. If there is a significant "pre-equilibrium" production, $\alpha_{c\bar{c}}$ becomes larger than 1.0.

Figure 4 shows p_t distribution of electron expected for central Au+Au collisions at RHIC. Momentum distribution of e^+ from various sources (π^0 Dalitz decay, decay of

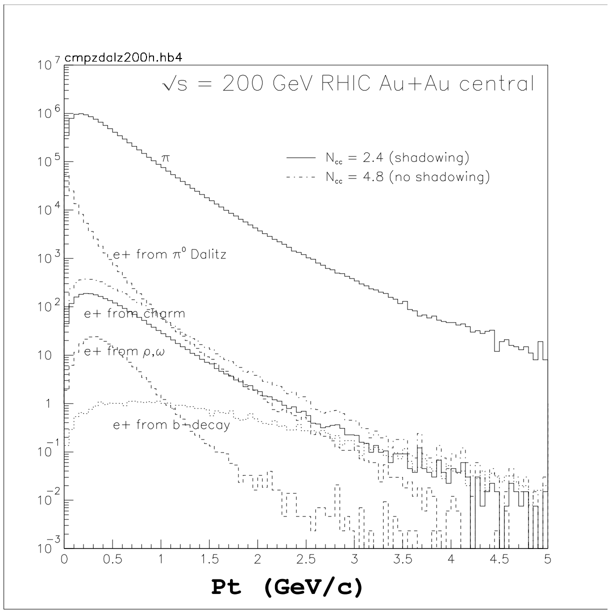

Figure 4. P$_t$ distributions of e^+ from π^0 Dalitz decays, from decay of charm and bottom quarks, and from decay of vector mesons in central Au+Au collision at RHIC. P$_t$ distribution of π^0 is also shown in the figure.

charm quark, ρ, ω, and bottom quark) are shown. In this calculation, we use the p_t distribution of π^0 based on the data from UA1 at $\sqrt{s} = 200$ GeV[52], and we use ISAJET 7.6 [53] to calculate p_t distribution of D and B mesons. The leptonic branching ratio of charm quark is assumed as 12 %, an average of Br($D^+ \to l^+X$) and Br($D^0 \to l^+X$). The figure shows two cases for charm e^+ spectrum, one for $N_{c\bar{c}} = 2.4$ and one for $N_{c\bar{c}} = 4.8$. The case $N_{c\bar{c}} = 4.8$ corresponds to $\sigma(pp \to c\bar{c}) = 160\mu b$ and $\alpha_{c\bar{c}} = 1.0$ with no nuclear shadowing, and the case $N_{c\bar{c}} = 2.4$ assumes a uniform 50 % suppression. Since there will be less nuclear shadowing at high p_t charm production[39,50], the latter underestimate the electron yield at high p_t. To evaluate bottom e^+ spectrum, we use the cross section $\sigma(pp \to b\bar{b}) = 2.5\ \mu b$ and $\alpha_{b\bar{b}} = 1.0$.

As one can see from the figure, the yield of charm decay e^+ is as large as that of π^0 Dalitz e^+ for p_t above 1.5 GeV/c. The e^+ from light vector meson decay is less than 10 % of charm e^+. For very high p_t (> 5 GeV/c), the contribution from the bottom decay can not be neglected.

The ratio $e^+(\text{charm})/\pi^0 \sim 5 \times 10^{-4}$ is several times higher than that observed at ISR energy, where the ratio "single e^+"/π is about 10^{-4} [54]. This larger value of e/π ratio is explained by two reasons. First, the charm production cross section at $\sqrt{s} = 200$ GeV is several times larger than that of ISR energy. Second, the charm cross section have larger nuclear dependence ($\alpha_{c\bar{c}} = 1.0$) than that of pions ($\alpha_\pi \sim 0.75$[55]) at mid-rapidity. Both effects favor larger c/π ratio, and thus larger e/π ratio, for Au+Au collisions at

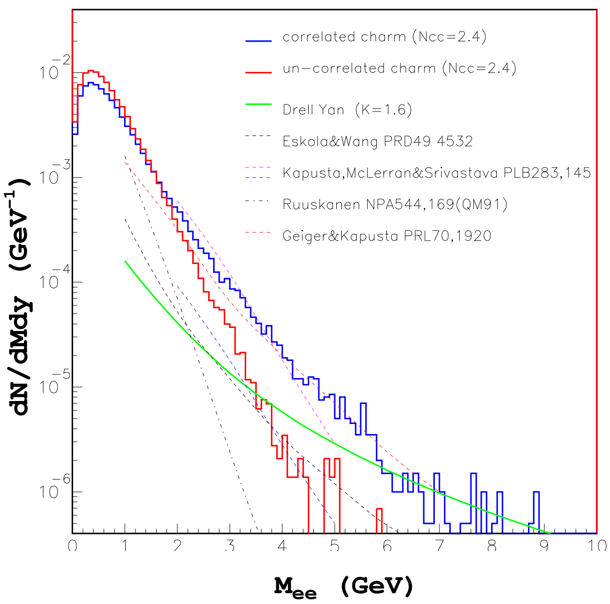

Figure 5. A dilepton mass distribution from charm decay and theoretical predictions of thermal dileptons.

RHIC compared with pp collisions at the ISR. If there is a significant $c\bar{c}$ production in "pre-equilibrium" stage of nucleus-nucleus collision, we expect an even larger e/π ratio.

We expect copious "single" electrons from charm decay in RHIC Au+Au collisions. The number of charm electrons with $p_t > 1$ GeV/c detected in PHENIX central arms is about 2×10^{-3} per central Au+Au collisions, or about 2 million per year. The measurement of "single" electron can be used as indirect measurement of charm production and its nuclear dependence.

6. Dilepton continuum and charm

The open charm is the major background for "thermal dilepton" continuum from the QGP. In figure 5, we compare the di-electron mass spectrum from charm decay and recent theoretical predictions of "thermal dilepton" mass distributions[56–59]. The mass spectrum from Drell-Yan process is also shown. The Drell-Yan cross section is evaluated with the K-factor 1.6, which reproduces the low energy data. We use $N_{c\bar{c}} = 2.4$ to calculate charm dilepton mass distribution.

There are two "charm dilepton" lines in the figure. One is that from "uncorrelated" charm leptonic decay, and the other is from "correlated" charm decay. The "correlated" charm di-electrons are produce by the process $gg(q\bar{q}) \rightarrow c\bar{c} \rightarrow e^+e^-X$, and it is proportional to the $c\bar{c}$ production. The "uncorrelated" charm dilepton is a pure combinatorial background of two e^+ and e^- from unrelated charm (anti-charm) decays. This background is proportional to $N_{c\bar{c}}^2$, and can not be neglected in high energy nucleus-nucleus collision.

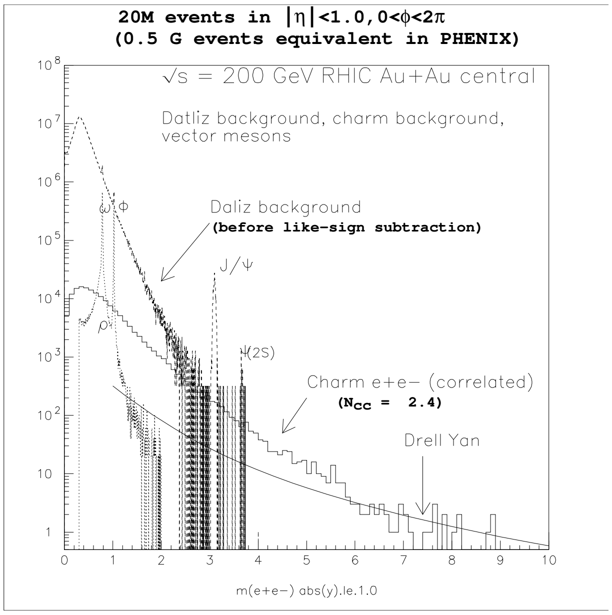

Figure 6. Dilepton mass distribution from Drell-Yan and charm decay compared with the vector meson signals and Dalitz/conversion backgrounds in PHENIX central detector.

However, the yield of the background can be estimated from link-sign pairs or from event mixing, and therefore it can be subtracted from the data.

The figure shows that the yield of "correlated" charm e^+e^- pairs are larger than that of Drell-Yan process below $M_{ee} = 6$ GeV, and larger than most of the theoretical predictions of dilepton continuum from QGP. In order to separate the thermal continuum, we need a direct measurement of charm dilepton spectrum. In PHENIX, this can be done by a measurement of $e^\pm - \mu^\mp$ pair using the central detector and the muon arm.

The "correlated" charm leptons have harder mass spectrum than that of "uncorrelated" charm lepton pairs. This is because the correlated pairs have strong back to back correlation, and tend to produce higher mass. It is possible that our calculation overestimates the momentum correlation of $c\bar{c}$ pair, and therefore the yield of charm dileptons in high mass region ($M_{ee} > 3$ GeV). The correlation can be reduced in collisions of heavy nucleus as c ($\bar{c}$) quark traverses through high density matter. We may be able to probe re-scattering/energy loss of c quarks from the angular correlations of charm dileptons.

Figure 6 shows the mass spectrum of Drell-Yan process, correlated charm dielectrons in $|y| < 1.0$. A mass spectrum of vector meson resonances and combinatorial background of π^0 Dalitz decays and γ conversions in PHENIX central arm is overlaid in the figure. The statistic of the figure is roughly equivalent to one year of data taking in PHENIX central arms. The figure shows that the charm dileptons is larger than Dalitz background above $M_{ee} \sim 3$ GeV.

7. Summary

We discussed on electron measurements in PHENIX detector at RHIC. Although we expect large Dalitz/conversion background in low mass region ($M_{ee} < 3$ GeV), we can clearly separate signals of narrow vector mesons (ω, ϕ) from the background. J/ψ is measured in $p_t < 6$ GeV/c. We discussed the consequence of large charm production expected in RHIC Au+Au collisions. The yield of charm decay electron is expected to be larger than Dalitz/conversion background for p_t above ~ 1.5 GeV/c. The lepton pairs from charm decay dominates over Drell-Yan process for mass as high as 6 GeV, and its yield is larger than most of theoretical predictions of thermal lepton pairs from QGP.

REFERENCES

1. PHENIX Conceptual Design Report, BNL 1993 (unpublished).
2. P. McGaughey, in these proceedings.
3. S. White, in these proceedings.
4. W. Zajc, in these proceedings.
5. Particle Data Group, Phys. Rev. D50 (1994) 1173.
6. R. D. Pisarski, Phys. Lett. 110B (1982) 155.
7. J. P. Blaizot and R. M. Galain, Phys. Lett. B271 (1991) 32.
8. G. E. Brown, Nucl. Phys. A522 (1991) 397c.
9. H. W. Barz, *et al.*, Phys. Lett. B265 (1991) 219.
10. P. Bi and J. Rafelski, Phys. Lett. B262 (1991) 485.
11. C. Gale and J. Kapusta, Nucl. Phys. B357 (1991) 65.
12. D. Lissauer and E. Shuryak, Phy. Lett. B253, (1991) 15.
13. C. M. Ko, P. Levai, X. J. Qju and C. T. Li, Phys. Rev. C45 (1992) 1400.
14. M. Asakawa, C. M. Ko, P. Levai, and X. J. Qiu, Phys. Rev. C46 (1992) R1159.
15. T. Hatsuda, Nucl. Phys. A544 (1992) 27c.
16. T. Hatsuda and S. H. Lee, Phys. Rev. C46 (1992) R34.
17. M. Asakawa and C. M. Ko, Rhys. Rev. C48 (1993) R526.
18. T. Hatsuda, Y. Koike, and S. H. Lee, Phys. Rev. D47 (1993) 1225.
19. C. A. Dominguez, M. Loewe and J. C. Rojas, Z. Phys. C59 (1993) 63.
20. C. M. Ko and D. Seibert, Phys. Rev. C49 (1994) 2198.
21. C. M. Ko and M. Asakawa, Nucl. Phys. A566 (1993) 447c.
22. S. Gupta, Nucl. Phys. A566 (1994) 69c.
23. M. Asakawa and C. M. Ko, Nucl. Phys. A572 (1994) 732.
24. U. Heinz and K. S. Lee, Nucl. Phys. A544 (1992) 503c.
25. PHENIX Conceptual Design Report Update, BNL 1994 (unpublished).
26. T. Åkesson *et al.*, Nucl. Phys. B203 (1982) 27.
27. T. Matsui and H. Satz, Phys. Lett. B178 (1986) 416.
28. M. C. Abreu *et al.*, Z. Phys. C38 (1988) 117.
    M. C. Abreu *et al.*, Nucl. Phys. A544 (1992) 209c.
29. M. C. Abreu *et al.*, Nucl. Phys. A566 (1994) 77c.
30. N. S. Craigie, Phys. Rep. 47 (1978) 1.
31. V. Barger and A. D. Martin, Phys. Rev. D31 (1985) 1051.
32. M. J. Leitch *et al.*, Nucl. Phys. A544 (1992) 197c.

33. C. Kourkoumelis *et al.*, Phys. Lett. 91B (1980) 481.
34. C. Ajbajar *et al.*, Phys. Lett. B200 (1988) 380.
    C. Ajbajar *et al.*, Phys. Lett. B256 (1991) 112.
35. F. Abe *et al.*, Phys. Rev. Lett. 69 (1992) 3704.
36. F. Karsch, Proceedings of the International Workshop on Quark Gluon Plasma Signatures, Strasbourg, France (1990).
37. E. W. N. Glover, F. Halzen, and A. D. Martin, Phys. Lett. B185 (1987) 441.
38. A. Shor, Phys. Lett. B215 (1988) 375.
    A. Shor, Phys. Lett. B233 (1989) 231.
39. B. Müller and X. N. Wang, Phys. Rev. Lett. 68 (1992) 2437.
40. Z. Lin and M. Gyulassy, NUCL-TH-9409007.
41. R. Vogt, B. V. Jacak, P. L. McGaughey, and P. V. Ruuskanen, Phys. Rev. D49 (1994) 3345.
42. M. Aguilar-Benitez *et al.*, Phys. Lett. B189 (1987) 476.
43. R. Ammar *et al.*, Phys. Rev. Lett. 61 (1988) 2185.
44. M. J. Leitch *et al.*, Phys. Rev. Lett. 72 (1994) 2542.
45. C. S. Mishra *et al.*, Phys. Rev. D50 (1994) R9.
46. K. Kodama *et al.*, Phys. Lett. B263 (1991) 573.
47. B. L. Combridge, Nucl. Phys. B151 (1979) 429.
48. M. L. Mangano, P. Nason, and G. Ridolfi, Nucl. Phys. B405 (1993) 507.
49. R. V. Gavai *et al.*, HEP-PH-9411438.
50. I. Sarcevic and P. Valerio, HEP-PH-9411317.
51. I. Sarcevic and P. Valerio, AZPH-TH/94-13.
52. C. Albajar *et al.*, Nucl. Phys. B335 (1990) 261.
53. H. Baer, F. E. Paige, S. D. Protopopescu, and X. Tata FSU-HEP-930329
54. F. W. Büsser *et al.*, Phys. Lett. 53B (1974) 212.
    F. W. Büsser *et a.*, Nucl. Phys. B113 (1976) 189.
55. W. M. Geist, Nucl. Phys. A525 (1991) 149c.
56. K. J. Eskola and X. N. Wang, Phys. Rev. D49 (1994) 4533.
57. J. Kapusta, L. McLerran, and D. K. Srivastava, Phys. Lett. B283 (1992) 145.
58. P. V. Ruuskanen, Nucl. Phys. A544 (1992) 169c.
59. K. Geiger and J. Kapusta, Phys. Rev. Lett. 70 (1993) 1920.